Hindawi
Journal of Chemistry
Volume 2023, Article ID 9845657, 1 page
https://doi.org/10.1155/2023/9845657

Retraction

Retracted: Experimental Study on Compressive Strength of Ultrahigh Performance Concrete Prefabricated Wall Structure

Journal of Chemistry

Received 15 August 2023; Accepted 15 August 2023; Published 16 August 2023

This article has been retracted by Hindawi following an investigation undertaken by the publisher [1]. This investigation has uncovered evidence of one or more of the following indicators of systematic manipulation of the publication process:

(1) Discrepancies in scope
(2) Discrepancies in the description of the research reported
(3) Discrepancies between the availability of data and the research described
(4) Inappropriate citations
(5) Incoherent, meaningless and/or irrelevant content included in the article
(6) Peer-review manipulation

The presence of these indicators undermines our confidence in the integrity of the article's content and we cannot, therefore, vouch for its reliability. Please note that this notice is intended solely to alert readers that the content of this article is unreliable. We have not investigated whether authors were aware of or involved in the systematic manipulation of the publication process.

Wiley and Hindawi regrets that the usual quality checks did not identify these issues before publication and have since put additional measures in place to safeguard research integrity.

We wish to credit our own Research Integrity and Research Publishing teams and anonymous and named external researchers and research integrity experts for contributing to this investigation.

The corresponding author, as the representative of all authors, has been given the opportunity to register their agreement or disagreement to this retraction. We have kept a record of any response received.

References

[1] J. Cao, Y. Dai, L. Hu, Y. luo, F. Long, and S. Ding, "Experimental Study on Compressive Strength of Ultrahigh Performance Concrete Prefabricated Wall Structure," *Journal of Chemistry*, vol. 2022, Article ID 3380144, 7 pages, 2022.

Hindawi
Journal of Chemistry
Volume 2022, Article ID 3380144, 7 pages
https://doi.org/10.1155/2022/3380144

Research Article

Experimental Study on Compressive Strength of Ultrahigh Performance Concrete Prefabricated Wall Structure

Jianfeng Cao,[1] **Yunfei Dai**,[1] **Liqiang Hu**,[1] **Yu luo**,[1] **Fang Long**,[1] **and Shiying Ding**[2]

[1]*Guangxi Xinfazhan Communications Group Co. Ltd., Nanning 530000, Guangxi, China*
[2]*Guangxi Road and Bridge Engineering Group Co. Ltd., Nanning 530000, Guangxi, China*

Correspondence should be addressed to Liqiang Hu; 1400440530@xs.hnit.edu.cn

Received 19 May 2022; Revised 5 June 2022; Accepted 9 June 2022; Published 23 June 2022

Academic Editor: K. K. Aruna

In order to study the influence of two parameters, height-thickness ratio and reinforcement ratio, on the compressive performance of prefabricated recycled concrete block-filled core walls, the author proposes a test method for the compressive strength of wall structures. In this method, 9 walls of dry and full-fill masonry are used, and the test measuring device and the arrangement of measuring points are designed to carry out the loading test. The results showed that reinforcement can significantly improve the axial compressive bearing capacity of the wall, but the out-of-plane displacement of the unreinforced wall is smaller than that of the reinforced wall. The larger the height-to-thickness ratio, the better the ductility of the reinforced core wall; the measured value of the axial compressive bearing capacity of the core-filled wall and the mean and coefficient of variation of the ratio to the standard calculated value were 1.49 and 0.13, respectively. The measured value is 34% to 68% higher than the standard calculated value. In conclusion, based on the test data and GB 50003–2011 "Code for Design of Masonry Structures," the theoretical calculation formula of the compressive bearing capacity of the prefabricated recycled concrete block-filled core wall is given.

1. Introduction

Since the 1920s, prefabricated buildings have become an important direction for the construction industry. In the 1960s, Britain, France, the Soviet Union, and other countries began to study and build prefabricated buildings. Since then, prefabricated buildings have developed rapidly and have been promoted around the world. Since 2015, my country has comprehensively promoted prefabricated buildings across the country, and there have been breakthroughs in recent years [1]. Prefabricated wall is an important part of prefabricated buildings, and it is widely used in prefabricated single buildings and fences. The prefabricated wall refers to the parts of the wall that are prefabricated by the factory and wall form for uniform installation at the construction site (Figure 1). The prefabricated wall is mainly constructed in the form of dry work, which has the advantages of short construction period, high efficiency, less labor, simple assembly, low manufacturing cost, and disassembly and reuse [2], it has a wide range of application prospects and has been widely explored at home and abroad, and many experiences are worth learning from.

At present, most of the rural houses in my country are mainly built by farmers, and there are many problems such as lack of effective earthquake resistance measures, uneven construction quality, and poor thermal insulation function. The prefabricated concrete structure has the advantages of low energy consumption, easy quality control, fast construction speed, good construction site environment, and less shrinkage cracks. To this end, the use of prefabricated concrete structures to build rural houses can effectively improve the construction quality of the house, save energy consumption, speed up construction, reduce construction waste, and fundamentally improve the quality of rural housing.

2. Literature Review

Meng X. et al. designed a precast concrete frame with welded and bolted joints, the low-cycle reciprocating load test was carried out with the cast-in-place concrete frame, and the

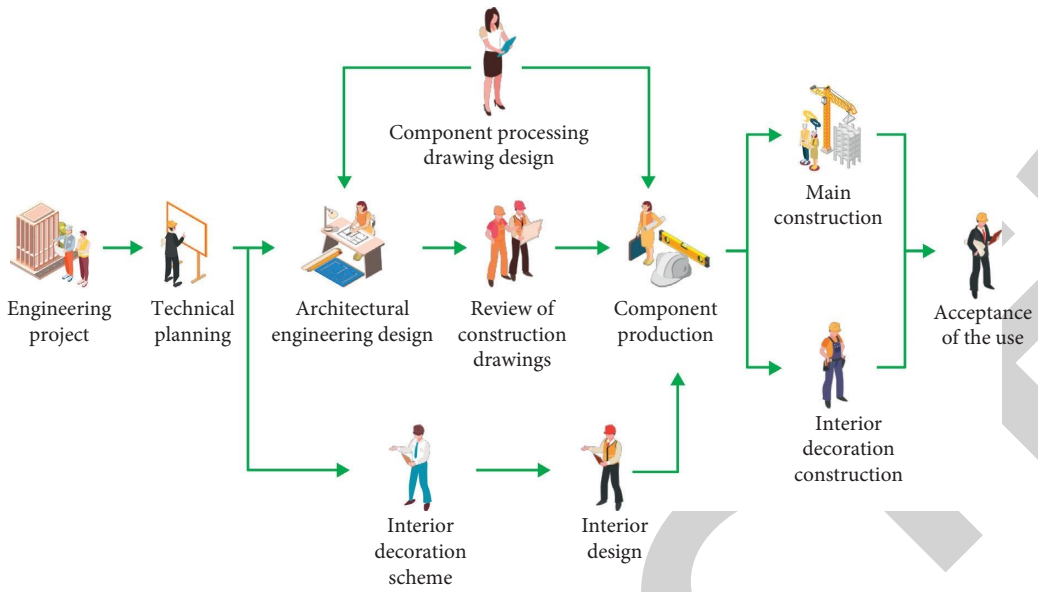

Figure 1: Assembly construction process.

responses of different connection types under the same loading mode were compared. It is shown that the improved bolted connection may be suitable for high-intensity areas [3]. Liu R. et al. conducted a low-cycle reciprocating loading test on composite plate shear wall specimens and cast-in-place specimens, and the result shows that, compared with the cast-in-place shear wall, the composite plate shear wall is slightly worse in stiffness degradation, and the stiffness degradation of the composite plate shear wall is more serious. Bonding properties between prefabricated wall panels and cast-in-place concrete are an important factor affecting the overall performance of the laminated plate shear wall, and the connection between the surface layers has less influence on it [4]. Jiang A. Q. et al. conducted axial and eccentric compression tests on 6 composite wallboards, combined with finite element analysis [5], and the test results showed that the overall performance of the laminated plate shear wall is better, the prefabricated layers on both sides are coordinated in force, and the bearing capacity increases with the increase of the slenderness ratio. Through the finite element modeling analysis, the bearing capacity formulas of the axial compression and eccentric compression of the laminated plate shear wall are given. Dai G. through a low-cycle reciprocating loading test study on a multilayer fabricated shear wall with vertical joints [6], considering factors such as horizontal longitudinal bars in vertical joints, shear keys in horizontal joints, and dowel bars in horizontal joints, studied its bearing capacity, stiffness, hysteresis, ductility, energy dissipation. The result showed that the ultimate bearing capacity of the fabricated shear wall specimen is related to the boundary constraints; when the shear key is set in the horizontal joint of the wall specimen, the setting of the dowel bar does not have a large effect on the peak point stiffness. Ding X. studied the finite element modeling of the fabricated shear wall structure and its seismic performance, and the finite element results show that setting vertical joints has little effect on the seismic performance of prefabricated shear walls. When designing vertical joints, the shear bearing capacity of the vertical joints should be calculated and analyzed [7]. Ismail S. et al. performed quasistatic loading on 4 hollow shear wall specimens connected by inserts, monotonic loading was carried out with two specimens, and extended analysis was carried out in combination with the finite element software ABAQUS. The result showed that the hollow form shear walls with single and double rows of inserted reinforcement meet the seismic requirements, and the seismic performance of the wall with double-row reinforcement is slightly better than that of the wall with single-row reinforcement; when the axial pressure is relatively large, the compression damage area of the wall increases [8].

Among the many studies, there are few studies on the mechanical properties of prefabricated recycled concrete block-filled core walls; therefore, it is of certain significance to study the mechanical properties of prefabricated recycled concrete block-filled core walls under axial compressive loads.

3. Research Methods

3.1. Dry Connection Prefabricated Wall Structure. The prefabricated panel structure by dry connectors (PPSDC) is proposed for rural housing. The structure is composed of prefabricated walls, prefabricated floor slabs, and prefabricated corner columns. For the vertical and horizontal joints of the wall, both are connected dryly, while the upper and lower corner posts are connected by grouting sleeves. There are two types of dry connections, bolted and welded. Due to the regular size and simple structure of prefabricated walls, it has the advantages of standardized design and industrialized production. At the same time, the four corners of the prefabricated floor slab are recessed inward to ensure that the prefabricated corner columns are connected up and down. The prefabricated corner columns are divided into

three cross-section forms, T-shaped, L-shaped, and cross-shaped, set at the intersection of vertical and horizontal walls to ensure the connection between vertical and horizontal walls and strengthen the force at the corners of the structure.

The dry joints of PSDC are divided into two types, vertical joints and horizontal joints, which are arranged in the connection area between the prefabricated components, and the prefabricated components are connected by steel connectors. Steel connectors are divided into two types: bolted connectors and welded connectors. Bolted connectors are composed of ordinary bolts and connecting steel plates, while welded connectors are composed of embedded steel sleeves and connecting steel plates.

3.2. Experimental Design

3.2.1. Test Material. The block used by the author is made by crushing and processing construction waste, and the block strength grade is MU10. The mix ratio of core-filled concrete refers to JC861-2000 "Small Hollow Block Concrete for Concrete," the strength grade of core-filled concrete is C20, the bottom beam and ring beam use ordinary concrete, and the strength class is C30.

3.2.2. Specimen Design and Production. A total of 9 wall specimens were used in the test, all of which were masonry with dry base and full filling [9]. The lowest one-skin block of the core-filled wall uses a sweeping block to simulate the masonry process of such a wall in an actual project. The core-filled wall is built without mortar, layer by layer, and the main masonry process [10, 11] is as follows: (1) Check whether the upper surface of the bottom beam is level with a laser line projection instrument. (2) According to the actual size of the wall, use the template as a corner to ensure the verticality of the wall. (3) During the dry laying of the wall, use a level to level the wide side of the wall. (4) After the 9 pieces of walls are all dry, check and calibrate the verticality of the walls with a laser line projector, and use wood to reinforce the adjacent 3 walls into a whole and restrict each other to prevent the wall from tilting when pouring the core concrete. (5) Consolidate self-compacting concrete with a strength grade of C20 to the wall holes. The height of the surface after the core concrete is poured, it should be about 3 cm lower than the height of the highest skin block of the core-filled wall, and a certain depth should be reserved to make the ring beam concrete and the core-filled wall mesh with each other. (6) After the initial setting of the core-filled concrete, fix the formwork and the holding angle of the ring beam together, and pour the ring beam concrete. (7) After 3 days, the core-filled wall is demolded, its surface is cleaned, and the core-filled wall specimen is masonry completed.

The specific design scheme of the test piece is shown in Table 1.

3.2.3. Test Measuring Device and Measuring Point Arrangement. A total of 6 strain gauges and 7 displacement sensors are arranged on the core-filled wall. Two strain gauges are, respectively, arranged on the two wide sides of the core-filled wall [12], and one strain gauge is arranged on the narrow sides, respectively, for physical alignment of the specimen during preloading. One displacement sensor is arranged at each of the upper, middle, and lower positions of the wide side, used to measure the out-of-plane displacement of the core-filled wall. Two displacement sensors are arranged on the two narrow sides, respectively, 2 displacement sensors inside, used to measure the axial deformation from the first skin block to the highest skin block at the bottom of the core-filled wall, and 2 displacement sensors on the outside, used to measure the axial displacement between the upper surface of the bottom beam and the bearing plate on the press. The wall reinforcement takes one wall as an example, and the odd-numbered skins of the core-filled wall are arranged with transverse reinforcement mesh.

3.2.4. Loading System. The test was carried out on a 20,000 kN press in a structural laboratory. The loading system is continuous loading; before the formal loading, the specimen is preloaded (10% estimated load) for 3 to 5 times; in the early stage of specimen loading, the control method of equipment loading is test force control, and the control loading rate is 2.0 ± 0.5 kN/s; when the load is applied to 70% of the estimated load, the control method of equipment loading is switched to displacement loading [13], the loading rate was maintained at 0.2 ± 0.01 mm/min, and the load increasing rate was not much different from that when the test force was controlled. The specific test steps are carried out in accordance with GB/T 50129–2011 "Standards for Test Methods of Basic Mechanical Properties of Masonry."

4. Analysis of Results

4.1. Destruction Analysis. The stress process of the 9 core-filled walls is basically similar; when the applied load is small, no cracks appear on the surface of the specimen, which is basically in the elastic working stage. When cracks appear in the core-filled wall, the specimen is considered to have entered the failure stage, and the failure process [14] is divided into three stages.

4.1.1. Stage 1. When the load is applied to the initial crack load of the wall, that is, 70% to 85% of the ultimate load, a vertical crack first appears on the upper part of the narrow side of the core-filled wall, there are no obvious cracks on the wide side, and this stage is regarded as the elastic-plastic stage of the core-filled wall.

4.1.2. Stage 2. Continue to load, the axial deformation of the specimen continues to increase, and a second vertical crack appears on the narrow side of the core-filled wall. The two main vertical cracks widened and developed downward. A few vertical cracks appeared at the vertical gray joints on the wide side of the core-filled wall. Explain the stress

Table 1: Specimen design scheme.

Specimen number	Number of test pieces (piece)	Dimensions (W × D × H) (mm)	Whether to reinforced	Test content
CW1-S	2	1018 × 100 × 1800	Yes	Research on the effect of height-thickness ratio on the compressive strength of walls
CW2-S	2	1008 × 100 × 1900	Yes	
CW3-S	2	1038 × 100 × 2300	Yes	
CW-4	1	1028 × 200 × 1600	No	Study on the effect of reinforcement ratio on the compressive strength of the wall
CW-5	1	1028 × 200 × 2000	No	
CW-6	1	1028 × 200 × 2400	No	

Note. The specimen number with the letter S is the reinforced wall; otherwise, it is the unreinforced wall.

concentration here. This stage is regarded as the plastic stage of the core-filled wall.

4.1.3. Stage 3. After the applied load reaches the ultimate load, the bearing capacity of the irrigated core wall decreases rapidly, the vertical cracks at the vertical ash joints on the wide side develop rapidly and penetrate the entire block, and the number of vertical cracks increases significantly. The corners of the blocks fall off, and the core-filled wall is brittle and broken. In the stage of decreasing compressive bearing capacity, the 2.4 m height of the irrigated core wall showed the phenomenon of block wall collapse, the block plays a good role in constraining the core column concrete, and the two could work well together.

4.2. Test Results. The 9 pieces of the core-filled wall all show the characteristics of brittle failure; with the increase of the height-to-thickness ratio of the core-filled wall, the axial deformation capacity of the wall increases, and the specific test data are shown in Table 2.

4.3. Wall Compressive Bearing Capacity. The author refers to GB 50003–2011 "Code for Design of Masonry Structures," the formula for calculating the compressive bearing capacity of the normal section of the reinforced block masonry member under axial compression [16], and the formula of the average compressive strength of the masonry; the calculation formula (1) of the axial compressive bearing capacity of the prefabricated recycled concrete block-filled core wall is derived [17]:

$$N = \phi\left(f_{gm}A + 0.8f'_y A'_s\right). \quad (1)$$

Here, $\phi = 1/(1 + 0.001\beta^2)$.

$$f_{gm} = k_1 f_1^{\alpha}(1 + 0.07f_2)k_2 + 0.63\delta\rho f_{cu,m}, \quad (2)$$

where N is the axial compressive bearing capacity of the core-filled wall; ϕ is the stability coefficient of the axial compression wall; f_{gm} is the average compressive strength of the perforated block masonry; A is the cross-sectional area of the core-filled wall; f'_y is the average compressive strength of the vertical reinforcement; A'_s is the cross-sectional area of all vertical reinforcement bars; β is the height-to-thickness ratio of the core-filled wall; f_1 is the average compressive strength of the block; α, k_1, and k_2 are all parameters related to the block, concrete block α takes 0.9, k_1 takes 0.46, the test blocks are mortar-free masonry, so f_2 is taken as 0, and k_2 is taken as 0.8; δ is the porosity of the block [18]; ρ is the porosity of the masonry; $f_{cu,m}$ is the average compressive strength of the porosity concrete cube.

Based on the test data, it is suggested that the formula for the axial compressive bearing capacity of the prefabricated recycled concrete block-filled wall is the following formula (3):

$$N = \phi\left(1.42f_{gm}A + 0.8f'_y A'_s\right). \quad (3)$$

In the formula, the calculation method of the parameters of ϕ and f_{gm} is the same as formula (1). Using formula (3) to calculate the axial compressive bearing capacity of the wall, the results are shown in Table 2.

It can be seen from Table 2 that the average value of the ratio of the measured value of the axial compressive bearing capacity of the core-filled wall to the calculated value in GB 50003–2011 and the coefficient of variation are 1.49 and 0.13, respectively. The measured value is 34%–68% higher than the calculated value in GB 50003–2011.

It can also be seen from Table 2 that the measured value of the axial compressive bearing capacity of the core-filled wall and the mean and coefficient of variation of the ratios to the values calculated by the proposed formula were 1.06 and 0.13, respectively. It shows that this suggested formula has a certain reference value.

4.4. Wall Load-Displacement Curve. According to the vertical displacement of the wall and the total load of the press measured by the displacement sensor [19], the following can be seen from Figures 2(a) and 2(b): (1) The data in the rising stage of the bearing capacity of the irrigated wall are in good agreement; after the ultimate load, the data are more discrete. The reason may be the brittle failure of the irrigated wall. On the other hand, it may be that the construction quality of the core-filled wall causes data dispersion. (2) Increasing the height-to-thickness ratio of the irrigated wall with steel reinforcements [20], its ductility is improved to a certain extent.

It can be seen from Figure 2(c) that the height-to-thickness ratio is the same, and the axial compressive bearing capacity of the reinforced wall, compared with the unreinforced wall, is increased by 11% to 15%.

4.5. Out-of-Plane Displacement-Load Curves of Walls. Out-of-plane displacement-load curves of 9-piece core-filled walls show the following: (1) As the height-to-thickness ratio

Table 2: Wall test results.

Specimen number	(Size) (mm)	Height-to-thickness ratio	(Fcr) (kN)	(Fm) (kN)	(Fn) (kN)	(Fc) (kN)
CW1-S-1	1032 × 200 × 1535	6.7	1400	2018	1874	2748
CW1-S-2	1050 × 200 × 1530	7.8	2150	2872	1974	2848
CW2-S-1	1042 × 200 × 1926	8.7	2520	2934	1945	2850
CW2-S-2	1050 × 200 × 1915	10.3	2300	3282	1945	2830
CW3-S-1	1043 × 200 × 2310	12.6	2900	3068	1866	3599
CW3-S-2	1046 × 200 × 2305	10.6	2040	3234	1766	5799
CW4	1051 × 200 × 1535	7.2	2450	2524	1788	3667
CW5	1039 × 200 × 1930	8.6	2130	2642	1901	2158
CW6	1030 × 200 × 2310	10.6	2560	2795	1819	2441

Note. (1) F_{cr} is the cracking load of the wall; F_m is the test value of the ultimate load of the wall; F_n is the ultimate load value of the wall calculated by the formula of the masonry code [15]; F_c is the theoretical value of the ultimate load of the wall calculated by the proposed formula. (2) The relative limit displacement is the relative displacement of the upper and lower measuring points on the narrow side of the wall under the ultimate load. (3) The compressive strength of the core-filled concrete is the average value of the compressive strength of three 150 mm^3 test blocks and the wall specimens after curing under the same conditions, which is about 20 MPa. (4) The block strength is the average compressive strength of the gross cross-sectional area of the five blocks after leveling, 8.54 MPa. (5) The specimen number with the letter S is a reinforced wall; otherwise, it is an unreinforced wall.

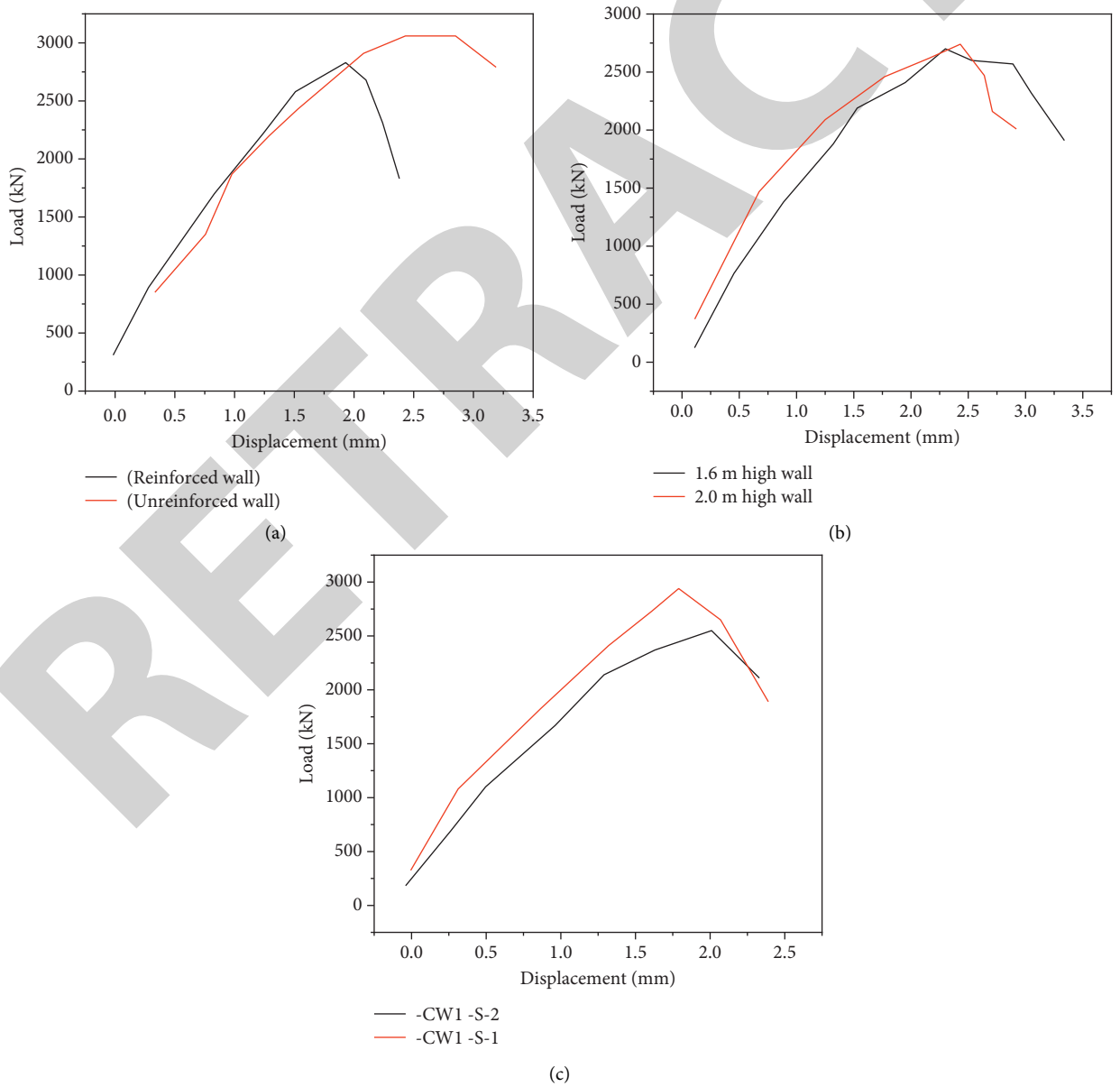

Figure 2: Wall load-displacement curve.

of the core-filled wall increases, the maximum out-of-plane displacement of the highest one-skin block under the ultimate load increases. (2) The out-of-plane displacement of the reinforced core wall is larger than that of the unreinforced core wall. (3) There is basically no out-of-plane displacement at the bottom of the core-filled wall, and the ratio of out-of-plane displacements in the middle and upper parts increases nonlinearly. (4) The maximum out-of-plane displacement of the highest skin block of the irrigated core wall is only 5 mm under the ultimate load, and this test is close to the axial compression test.

4.6. Design Principles of PPSDC Ductile Nodes. From the analysis of the above failure mechanism and test results, it can be seen that the failure area of PPSDC is mainly concentrated in the node area at the bottom of the structure, and the failure mode is different from the cast-in-place structure or the equivalent cast-in-place fabricated structure [21]; the existing seismic methods of concrete structures cannot be used for design; therefore, it is necessary to establish the PPSDC calculation theory and ductility design concept based on joint performance.

The results showed that the failure mode of the bolted structure is the punching failure of the concrete around the bolts in the bottom node area. The failure mode of the welded connection structure is the anchor failure of the steel embedded parts at the bottom of the wall. Both failures are dry joint failures and belong to the brittle failure mode, and the realization of the expected ductile failure mode under earthquake action is one of the main factors in ensuring the seismic performance of the structure. Therefore, in order to realize the ductile failure of PPSDC, the plasticity of the connecting steel plate should be fully utilized, ensure punching failure of concrete and anchor failure of steel embedded parts, and not occur before yielding of the connecting steel plates, improving the ductility of dry joints [11].

Therefore, the design principle of ductile joints of PPSDC is proposed as "strong anchorage, strong surrounding, and weak steel plate." The purpose is to take advantage of the good ductility of steel connectors, the connecting steel plate is selected as the main energy-consuming component, and in order to make the failure first occur at the connecting steel plate, the hinge-out sequence, damage degree, and energy-dissipation mechanism of the plastic hinges in different parts of the dry joint area should be controlled properly. In order to ensure that there will be no concrete punching failure in the node area, anchor failure of the steel embedded parts should be avoided. Only by achieving this, the ductile failure mode of the structure can be realized. For bolted connection structures, the punching shear resistance of the concrete in the node area can be enhanced by increasing the minimum end distance and minimum side distance of the bolt holes of the wall panel or using new materials such as high ductility concrete to improve the brittle performance of the node area. For welded connection structures, the connection between anchor bars and steel embedded parts can be improved, such as the use of threaded connections, in order to improve the anchoring capacity of steel embedded parts in the wall.

5. Conclusion

Through the experimental study and analysis of the mechanical properties of the 9-piece prefabricated recycled concrete block-filled wall under axial load, the following conclusions can be drawn:

(1) The axial compression limit load of the reinforced wall is 11% to 15% higher than that of the unreinforced wall; due to the effect of the internal reinforcement of the core-filled wall, the out-of-plane displacement of the highest block of the reinforced wall is larger than that of the unreinforced wall.

(2) Increase the height-to-thickness ratio of the reinforced prefabricated recycled concrete block-filled wall; its ductility is improved to a certain extent.

(3) Based on the suggested formula given in GB 50003–2011 and test data, it can be used to calculate the axial compressive bearing capacity of the prefabricated recycled concrete block-filled wall, and the experimental values are in good agreement with the calculated results.

Data Availability

The data used to support the findings of this study are available from the corresponding author upon request.

Conflicts of Interest

The authors declare that they have no conflicts of interest.

Acknowledgments

This study was supported by the Ningbo Transportation Technology Plan (202110), Science and Technology Program of Zhejiang Provincial Communications Department (no. 2019040).

References

[1] C. L. Wang, S. Jiang, B. C Li, and S. Li, "Research on mechanical properties of a new fabricated wall material in building with light steel structure," *Materials Science Forum*, vol. 1001, pp. 145–154, 2020.

[2] V. K. Dragunov, A. P. Sliva, A. L. Goncharov et al., "Specific features of electron-beam welding of iter blanket first wall components," *Thermal Engineering*, vol. 67, no. 6, pp. 387–395, 2020.

[3] X. Meng, K. Liu, Z. Li, and L. Sha, "Experimental study on seismic performance of prefabricated beam wall out-of-plane connection nodes with different anchoring measures," *KSCE Journal of Civil Engineering*, vol. 26, no. 2, pp. 770–780, 2021.

[4] R. Liu, H. Huang, Z. Sun, A. Alexander-Katz, and C. A. Ross, "Metallic nanomeshes fabricated by multimechanism directed self-assembly," *ACS Nano*, vol. 15, no. 10, pp. 16266–16276, 2021.

[5] A. Q. Jiang, W. P. Geng, P. Lv, J. W. Hong, and C. S. Hwang, "Ferroelectric domain wall memory with embedded selector realized in linbo3 single crystals integrated on si wafers," *Nature Materials*, pp. 1–7, 2020.

[6] G. Dai, J. Zhu, Y. Song, S. Li, and G. Shi, "Experimental study on the deformation of a cut-off wall in a landfill," *KSCE Journal of Civil Engineering*, vol. 24, no. 5, pp. 1439–1447, 2020.

[7] X. Ding, Z. Chen, and M. Xu, "Shaking table experiment of a recycled concrete block masonry building structure with a 'self-contained' structural system," *Advances in Structural Engineering*, vol. 24, no. 3, pp. 422–436, 2020.

[8] S. Ismail and M. Ramli, "Resistance to chloride penetration of recycled aggregate concrete modified using treated coarse recycled concrete aggregate and fibres," *Materials Science Forum*, vol. 991, pp. 101–108, 2020.

[9] T. Meng, J. Zhang, H. Wei, and J. Shen, "Effect of nano-strengthening on the properties and microstructure of recycled concrete," *Nanotechnology Reviews*, vol. 9, no. 1, pp. 79–92, 2020.

[10] S. Ismail and M. Ramli, "Mechanical properties of concrete using treated recycled concrete aggregate in marine environment," *Key Engineering Materials*, vol. 841, pp. 138–143, 2020.

[11] C. Hui, K. Li, Y. Li, Y. Bian, R. Hai, and C. Li, "Experimental study and analysis on axial compression performance of high-strength recycled concrete-filled steel tube column in corrosive environments," *International Journal of Steel Structures*, vol. 22, no. 2, pp. 450–471, 2022.

[12] G. Balasubramanian, "Manufacture of concrete paver blocks with recycled demolition waste," *Electronic Journal of Structural Engineering*, vol. 20, no. 1, pp. 78–82, 2020.

[13] N. C. Ugochukwu, A. Eguakhide, A. V. Sunday, and O. E. Chinonso, "Performance of lightweight interlocking pavement concrete block composite made from breadfruit shell ash particle and momordica angustisepala fiber via modified casting method," *International Journal of Advanced Manufacturing Technology*, vol. 116, pp. 1–11, 2021.

[14] K. Sharma and B. K. Chaurasia, "Trust based location finding mechanism in VANET using DST," in *Proceedings of the 5th International Conference on Communication Systems & Network Technologies*, Piscataway, NJ, USA, 2015.

[15] M. S. Pradeep Raj, P. Manimegalai, P. Ajay, and J. Amose, "Lipid data acquisition for devices treatment of coronary diseases health stuff on the internet of medical things," *Journal of Physics: Conference Series*, vol. 1937, no. 1, 2021.

[16] X. Liu, J. Liu, J. Chen, F. Zhong, and C. Ma, "Study on treatment of printing and dyeing waste gas in the atmosphere with Ce-Mn/GF catalyst," *Arabian Journal of Sciences*, vol. 14, no. 8, pp. 1–6, 2021.

[17] R. Huang, S. Zhang, W. Zhang, and X. Yang, "Progress of zinc oxide-based nanocomposites in the textile industry," *IET Collaborative Intelligent Manufacturing*, vol. 3, pp. 281–289, 2021.

[18] K. Yang, L. Yang, P. Gong, L. Zhang, Y. Yue, and Q. Li, "Experiment and analysis of mechanical properties of carbon fiber composite laminates under impact compression," *E-Polymers*, vol. 22, no. 1, pp. 309–317, 2022.

[19] X. K. Yan, S. Zhang, G. L. Zhao, X. Chen, and B. Zhang, "Experimental study on the influence of second-order effect on shear bearing capacity of frame columns with cracks under different axial compression ratios," *Materials Science Forum*, vol. 1020, pp. 93–103, 2021.

[20] S. Lagen, L. Giupponi, A. Hansson, and X. Gelabert, "Modulation compression in next generation ran: air interface and fronthaul trade-offs," *IEEE Communications Magazine*, vol. 59, no. 1, pp. 89–95, 2021.

[21] C. Wang and R. Liu, "Dynamic ultimate bearing capacity of beam-plate coupled structures with deformable connection under uniaxial compression, compression-bending and compression–shear loadings," *Archive of Applied Mechanics*, vol. 91, no. 7, pp. 1–21, 2021.